Geophysical Research Letters

RESEARCH LETTER
10.1029/2022GL100453

Oceanic Electrical Conductivity Variability From Observations and Its Budget From an Ocean State Estimate

D. S. Trossman[1,2,3] **and R. H. Tyler**[4,5]

[1]Earth System Science Interdisciplinary Center, University of Maryland, College Park, MD, USA, [2]Department of Oceanography and Coastal Sciences, Louisiana State University, Baton Rouge, LA, USA, [3]Center for Computation & Technology, Louisiana State University, Baton Rouge, LA, USA, [4]Geodesy and Geophysics Laboratory, NASA Goddard Space Flight Center, Greenbelt, MD, USA, [5]Goddard Earth Science and Technology Research (GESTAR) II, University of Maryland, Baltimore County, MD, USA

Abstract Because spatio-temporal variations in ocean heat content (OHC) are strongly predicted by ocean conductivity content (OCC) over most of the global ocean, we analyze the dynamical budget and behavior of the electrical conductivity of seawater. To perform these analyses, we use an ocean-model state estimate designed to accurately represent long-term variations in ocean properties in a dynamically and kinematically consistent way. We show that this model accurately reproduces the spatio-temporal variations in electrical conductivity seen in satellite-derived data and in a seasonal climatology product derived from in-situ data, justifying use of the model data to perform further analyses. An empirical orthogonal function analysis suggests that the vast majority of the variance in OHC and OCC can be explained by similar mechanisms. The electrical conductivity budget's most important term is the temperature forcing tendency term, suggesting that ocean heat uptake is the mechanism responsible for the strong relationship between OCC and OHC.

Plain Language Summary The ocean conducts electricity because it contains charged particles. While the dynamical budget and behavior of ocean temperature and salinity have been well studied, similar basic analyses have not been conducted for ocean conductivity. The goal of this study is to provide this using realistic ocean conductivity data describing spatial and temporal variations. Providing a realistic description of conductivity and its dynamical variability is motivated by recent interest in using in-situ and remote estimates of ocean conductivity content (OCC) to infer ocean heat content (OHC). The latter is both highly important in understanding climate change and inadequately observed using traditional methods. The primary result of this study is that, in most of the global ocean, both spatial and temporal variability in OHC are strongly predicted by OCC through ocean heat uptake, raising the importance of developing electric and magnetic methods for monitoring OCC and thereby OHC by proxy.

Key Points:

- Close agreement between observationally derived and Estimating the Circulation & Climate of the Ocean-calculated conductivity
- Temperature forcing tendency term dominates electrical conductivity budget
- Conductivity can be locally influenced by advection of temperature (low-latitudes) and salinity (high-latitudes)

Supporting Information:

Supporting Information may be found in the online version of this article.

Correspondence to:

D. S. Trossman,
david.s.trossman@gmail.com

Citation:

Trossman, D. S., & Tyler, R. H. (2022). Oceanic electrical conductivity variability from observations and its budget from an ocean state estimate. *Geophysical Research Letters*, *49*, e2022GL100453. https://doi.org/10.1029/2022GL100453

Received 14 JUL 2022
Accepted 8 SEP 2022

Author Contributions:

Conceptualization: D. S. Trossman
Data curation: D. S. Trossman
Formal analysis: D. S. Trossman
Funding acquisition: D. S. Trossman, R. H. Tyler
Investigation: D. S. Trossman
Methodology: D. S. Trossman
Project Administration: D. S. Trossman
Resources: D. S. Trossman
Software: D. S. Trossman, R. H. Tyler
Supervision: D. S. Trossman
Validation: D. S. Trossman
Visualization: D. S. Trossman
Writing – original draft: D. S. Trossman
Writing – review & editing: D. S. Trossman, R. H. Tyler

1. Introduction

While electrical conductivity is a fundamental parameter in the electrodynamics of the ocean, in the more typical fields of physical oceanography treating fluid dynamics and thermodynamics, electrical conductivity is usually only discussed as a proximate variable for conveniently obtaining salinity. Conductivity is indeed much easier to measure than salinity directly. In fact, ocean salinity has become defined by referencing observations of electrical conductivity of a seawater sample to that of a potassium chloride solution under standardized temperature and pressure conditions (UNESCO, 1985). At a given pressure, the electrical conductivity of the ocean alone does not provide sufficient information to associate it with a unique combination of temperature and salinity. However, given two of the three (electrical conductivity, temperature, and salinity), the third can be uniquely determined, despite their nonlinear relationship.

Because salinity is required to estimate the dynamically important density, conductivity has been extensively measured in the ocean to high accuracy. However, the conductivity data itself has not typically been archived. Rather, it must be estimated from the archived temperature and salinity co-observations. This approach was followed in developing the first "climatology" data set for ocean conductivity (Tyler et al., 2017), which has since been updated in Reagan et al. (2019). Climatology data sets (long available for temperature and salinity) refer to gridded data products constructed from an objective analysis of the many observations. The latest World Ocean Atlas (2018) (WOA18) data in Reagan et al. (2019) provides global ocean conductivity at 0.25° (latitude

and longitude) resolution and 102 standard levels spanning the ocean depth. This data includes sets (used in the present study) describing the temporal mean as well as each of the four seasons. Further, satellite derived sea surface temperature and salinity observations provide some information about the interannual variability in sea surface conductivity.

While conductivity depends on both temperature and salinity, an interesting finding in the climatology data (Tyler et al., 2017) was that the depth-average of conductivity is strongly related to that of temperature, motivating further studies which have found support for using depth-integrated conductivity ("ocean conductivity content" (OCC)) to predict depth-integrated heat ("ocean heat content" (OHC)) (Trossman & Tyler, 2019; Irrgang et al., 2019; Trossman & Tyler, 2022). Of course depth-integrated parameters can show strong spatial co-variability simply due to the common depth and the relationships referred to here involve either depth-averaged variables or covariability beyond what can be simply explained by depth. The goal of the present study is to describe conductivity data sets that contain realistic spatial and temporal variability and apply this to elucidating the dynamical reasons for the high covariability between OCC and OHC.

A second reason for describing the realistic behavior of ocean conductivity is that this data is needed in forward models of ocean electrodynamics. The ocean is pervaded by large-scale electric currents generated by induction (involving excitation by field sources in the ionosphere and magnetosphere; e.g., Kuvshinov (2008)) and motional induction (due to the motion of the electrically-conducting fluid, such as the ocean, through the Earth's main magnetic field), which have associated local and remote magnetic fields (e.g., Manoj et al., 2006; Sanford, 1971; Stephenson & Bryan, 1992; Tyler et al., 1997). At periods much greater than 10 min [Tyler, 2017), even the thickest regions of the ocean are "electrically thin," meaning the electromagnetic wavelength/attenuation scale inside the ocean is much smaller than the ocean thickness and therefore the horizontal electric currents excited are approximately depth-independent. Hence, the ocean's external magnetic field depends on OCC rather than surface electrical conductivity. However, due to the insufficient spatio-temporal sampling of the full-depth observations of electrical conductivity, our knowledge of the interannual variability in the subsurface ocean's electrical conductivity is lacking, which is one focus of the present study.

No previous study has balanced a tracer tendency equation for the ocean's electrical conductivity, in which each physical factor impacting the electrical conductivity has its time-rate of change quantified and balanced with the total time-derivative (referred to as a "budget" hereafter). However, there are numerous studies that have evaluated these types of budgets for ocean heat, salt, and (steric) sea level. For example, using an observationally-constrained but dynamically and kinematically consistent ocean state estimate, Piecuch and Ponte (2011) showed that the interannual variations in sea level are primarily associated with steric sea level and that variations in steric sea level are mostly due to advection in the tropical Indian and Pacific oceans and both advection and diffusion at extratropical latitudes, with local surface buoyancy fluxes contributing in relatively few regions. Using a free-running coupled climate model, Palter et al. (2014) found diffusion to be more important to steric sea level variability on a global-mean scale than Piecuch and Ponte (2011), at least when considering vertical versus lateral diffusion separately, but their results otherwise qualitatively agree. Piecuch and Ponte (2014) further demonstrated that the global-mean steric sea level trend is set by surface heat and freshwater exchanges that are primarily offset by the redistribution of heat and salt through advection and diffusion, which generally agrees with the results of Palter et al. (2014). The relative roles of temperature and salinity variability associated with different physical processes in determining the electrical conductivity variability remain unknown.

The modeling system used to generate the electrical conductivity budget data analyzed here (a run of the Estimating the Circulation & Climate of the Ocean (ECCO) framework (Fukumori et al., 2017) from 1992 to 2015 without having to optimize the model's free parameters again, a "re-run") is described in the following section. Essentially, the optimized run of ECCO solves for the initial conditions, model parameters, and forcing fields using an adjoint-based data assimilation method. These estimates are then utilized in a forward simulation (the re-run) with new diagnostics (e.g., each tendency term in the electrical conductivity budget, broken up by temperature and salinity contributions) saved as model output. There are at least three strengths in using ECCO to assess whether OHC can be predicted from OCC. First, model output is more globally complete than observational data sets in both time and space. Second, ECCO has been validated against several independent data sets (Forget, Campin, et al., 2015; Heimbach et al., 2019). Third, its re-run is guaranteed to maintain consistency in the dynamics and physics of its underlying ocean model, which filter-based reanalyzes cannot do due to their use of analysis increments (Pilo et al., 2018; Stammer et al., 2016).

In this study, we consider how advection, diffusion, and forcings of heat and salt determine the variability in electrical conductivity using a more updated version of the same ocean state estimation framework as Piecuch and Ponte (2011). We organize this manuscript as follows. In Supporting Information S1, we describe the observations simply which we use to assess how realistic the ECCO state estimate's output is and the observation-model comparisons. In the main text, we describe ECCO and the conductivity budget. We then describe the analysis of what explains the variability in depth-integrated electrical conductivity and other correlates, and the conductivity budget results. We lastly make concluding remarks for the consequences of our findings and for future research.

2. Model Description and Budget Framework

2.1. Modeling System

The modeling system used here is the ECCO-Production version 4 revision 3 (ECCO-Production ver4.rev3 or ECCOv4r3) run, which was accomplished and described by Fukumori et al. (2017). The same framework was used by Trossman and Tyler (2019, 2022), but is described again here. The underlying ocean-sea ice model for ECCOv4r3 is based on the Massachusetts Institute of Technology general circulation model (MITgcm), which is a global finite volume model. The ECCOv4r3 global configuration uses curvilinear Cartesian coordinates (Forget, Campin et al. (2015)—see their Figures 1–3) at a nominal 1° (0.4° at equator) resolution and rescaled height coordinates (Adcroft & Campin, 2004) with 50 vertical levels and a partial cell representation of bottom topography (Adcroft et al., 1997). The MITgcm uses a dynamic/thermodynamic sea ice component (Heimbach et al., 2010; Losch et al., 2010; Menemenlis et al., 2005) and a nonlinear free surface with freshwater flux boundary conditions (Campin et al., 2004). The wind speed and wind stress are specified as 6-hourly varying input fields over 24 years (1992–2015). Average adjustments to the wind stress, wind speed, specific humidity, shortwave downwelling radiation, and surface air temperature are re-estimated and then applied over 14-day periods. These adjustments are based on estimated prior uncertainties for the chosen atmospheric reanalysis (Chaudhuri et al., 2013), which is ERA-Interim (Dee et al., 2011). The net heat flux is then computed via a bulk formula (Large & Yeager, 2009). The ocean variables, on the other hand, do not get periodically adjusted. A parameterization of the effects of geostrophic eddies (Gent & McWilliams, 1990) is used. Mixing along isopycnals is accounted for according to the framework provided by Redi (1982). Vertical mixing is the sum of diapycnal mixing and the vertical component of the along-isopycnal tensor, where diapycnal mixing is determined according to the Gaspar et al. (1990) mixed layer turbulence closure and estimated background diapycnal diffusivity. Convective adjustment does not act through the diapycnal diffusivity in the MITgcm. Here, the model's diapycnal diffusivity represents a combination of processes, including–but potentially not limited to–internal wave-induced mixing. The background diapycnal diffusivity, the Redi coefficient, and the Gent-McWilliams coefficient are time-independent because of the under-determined problem of inverting for initial conditions and model parameters would be even more under-determined if they were allowed to vary in time. The electrical conductivity is calculated using the TEOS-10 package (McDougall & Barker, 2011) as the model runs by solving for the in-situ temperature based on the simulated potential temperature.

The objective of the optimized ECCOv4r3 solution is to minimize the cost function, which is a combination of (a) a weighted sum of squares of the disagreements between the model and observations and (b) a sum of penalties that do not appear in the estimation itself but push control variables toward certain parts of the control space. The least-squares problem solved by the ECCO model uses the method of Lagrange multipliers through iterative improvement, which relies upon a quasi-Newton gradient search (Gilbert & Lemarechal, 1989; Nocedal, 1980). Algorithmic (or automatic) differentiation tools (Griewank, 1992; Giering & Kaminski, 1998) have allowed for the practical use of Lagrange multipliers in a time-varying non-linear inverse problem such as ocean modeling, eliminating the need for discretized adjoint equations to be explicitly hand-coded. Contributions of observations to the model-data misfit function are weighted by best-available estimated data and model representation error variance (Wunsch & Heimbach, 2007). The observational data included in the ECCO state estimation procedure are discussed in Forget, Campin et al. (2015) and Fukumori et al. (2017). These data include satellite derived ocean bottom pressure anomalies, sea ice concentrations, sea surface temperatures, sea surface salinities, sea surface height anomalies, and mean dynamic topography, as well as profiler- and mooring derived temperatures and salinities (Fukumori et al., 2017) (see their Table 3). The control variables that are inverted for iteratively by ECCO include the initial condition of the velocities, sea surface heights, temperatures, and salinities; time-mean three-dimensional Redi (Redi, 1982) coefficients, Gent-McWilliams (Gent & McWilliams, 1990) coefficients,

and vertical diffusivities (Gaspar et al., 1990); and time-varying two-dimensional surface forcing fields. The error covariances for each of the ocean subgrid-scale transport and mixing parameters are specified by imposing a smoothness operator (Weaver & Courtier, 2001) at the scale of three grid points–decorrelation length scale diameter of ∼100 km–which allows for the dynamical model to regionally adjust from the information provided by observations (Forget, Ferreira, & Liang, 2015). Fifty-nine iterations of the parameter and state estimation procedure–the "optimization" run–were performed to arrive at the ECCOv4r3 solution, which we use for initial conditions and model parameters in our experiments.

2.2. Electrical Conductivity Budget

In order to examine the importance of particular processes to variations in electrical conductivity (σ) we analyze a modified version of ECCOv4r3's temperature and salinity budgets to calculate the electrical conductivity budget. In other words, we calculate the instantaneous time-rate of change in electrical conductivity, $\partial\sigma/\partial t$, and each physical process that affects the electrical conductivity for each model time step. The tracer equation terms required for the potential temperature (Θ) budget are related to those for the electrical conductivity budget by multiplying by $\partial\sigma/\partial\Theta$ and the tracer equation terms required for the salinity (S) budget are related to those for the electrical conductivity budget by multiplying by $\partial\sigma/\partial S$. Each of these terms are computed online and saved as the model runs. That is, we compute the terms in the electrical conductivity budget inline before saving them as model output instead of calculating these fields offline from averaged model output of time-derivatives in temperature and salinity because the chain rule is applied to get time-derivatives in electrical conductivity. Finally, the monthly averages of the resulting electrical conductivity terms are saved to the output files used in this analysis.

The tracer equations can be broken down into "tendency" terms (i.e., individual contributions to the time derivative of the oceanic tracer) (Palter et al., 2014),

$$\begin{aligned} \rho\frac{d\Theta}{dt} &= -\nabla\cdot\mathbf{J}^{\Theta} + \rho Q^{\Theta} \\ \rho\frac{dS}{dt} &= -\nabla\cdot\mathbf{J}^{S} + \rho Q^{S}, \end{aligned} \tag{1}$$

where $d/\mathrm{dt} = \partial/\partial t + (\mathbf{v} + \mathbf{v}^*)\cdot\nabla$ is the material derivative, $\mathbf{v}$ is the resolved velocity field, $\mathbf{v}^*$ is the eddy-induced or quasi-Stokes velocity field that represents parameterized motions, Θ is the potential temperature, S is the salinity, ρ is the locally referenced potential density, $\mathbf{J}^{\Theta}$ and $\mathbf{J}^{S}$ are the fluxes associated with the parameterized mixing along constant density surfaces ("along-isopycnal diffusivities") and across constant density surfaces ("diapycnal diffusivities") for potential temperature and salinity, and Q^{Θ} and Q^{S} are the sums of sources and sinks of potential temperature and salinity.

The potential temperature and salinity budget terms summarized by Equation 1 are computed as follows. The resolved and mesoscale transports are accounted for in the material derivatives Θ and S, and the along-isopycnal and diapycnal diffusion of Θ and S are accounted for by $\mathbf{J}^{\Theta}$ and $\mathbf{J}^{S}$. The diapycnal diffusion term is added to the vertical component of the along-isopycnal diffusion term, which is against convention (e.g., Palter et al. (2014)). Shortwave radiation flux is allowed to penetrate down to 200 m in an exponentially decaying manner (Paulson & Simpson, 1977). The sources and sinks of Θ and S accounted for by Q^{Θ} and Q^{S} include surface buoyancy fluxes (latent, sensible, shortwave, and longwave); geothermal heat flux from hydrothermal vents at the seafloor; precipitation minus evaporation; freshwater fluxes from land ice; and formation of frazil ice (which occurs under turbulent conditions to produce randomly oriented loose crystals that don't float in water).

3. Results

The high level of agreement between ECCOv4r3 and observations (see Supporting Information S1; Figures S1–S3 in Supporting Information S1) justifies using the ECCOv4r3 data for the remainder of this study. Unlike the observational comparisons, when we refer to OCC, OHC, and ocean salinity content (OSC), hereafter, we are referring to full depth-integrated quantities. We present the temporally-averaged OCC, its spatial gradients, and depth-averaged equivalents (Figure S4 in Supporting Information S1) and their temporal variability (Figure S5 in Supporting Information S1) over the length of the ECCOv4r3 simulation (1992–2015) in Supporting Information S1 for reference.

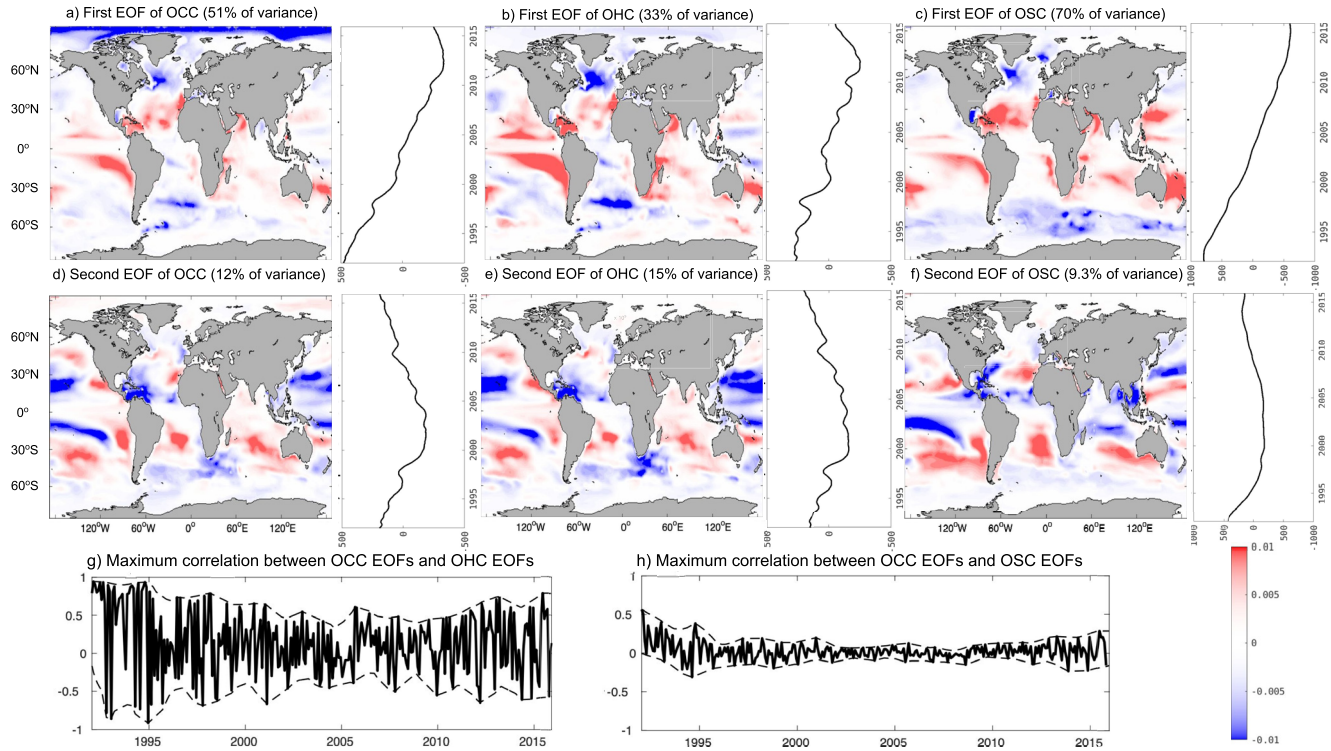

Figure 1. The first (panels a–c) and second (panels d–f) empirical orthogonal functions for area-weighted and normalized (scaled by standard deviations of) ocean conductivity content (OCC—panels a and d), ocean heat content (OHC—panels b and e), and ocean salt content (OSC—panels c and f). The time series next to each corresponding EOF map are the corresponding Principal Components as functions of time. The units are dimensionless in panels a–f. Also shown are the maximum canonical spatial correlations (black solid curves) and the low-passed filtered envelopes of these correlations (black dashed curves) between the OCC EOFs and OHC EOFs as a function of EOF number (panel g) and between the OCC EOFs and OSC EOFs as a function of EOF number (panel h).

3.1. Covariability of OCC, OHC, and OSC in ECCOv4r3

Using the ECCOv4r3 output from our new simulations, we investigate the covariability between OCC, OHC, and OSC. We perform an empirical orthogonal function (EOF) decomposition of each field after removing each of their means (Figure 1) and extend this to a multivariate EOF analysis in Supporting Information S1 to demonstrate the spatial patterns of covariability in OCC and OHC (Figure S6 in Supporting Information S1). We area-weight each field and normalize them by their standard deviations prior to calculating the EOFs. The first EOF for OHC and the first EOF for OCC are related to ocean warming (Figures 1a and 1b) and explain between one-third and one-half of each of their variances. The first EOF for OSC is related to land ice melt (Figure 1c) and explains 60% of the variance. The second EOF for OHC and the second EOF for OCC are related to natural climate variability (Figures 1d and 1e) such as the El Niño Southern Oscillation, consistent with previous analyses that used observations of only the upper 700 m (e.g., Wang et al. (2020)). The second EOF for OSC is related to sea ice melt and evaporation minus precipitation trends (Figure 1f). While the OCC, OHC, and OSC tend to be highly correlated regardless of season and it is unclear whether any EOF beyond the second has a physical interpretation (not shown), the first several EOFs for OHC and OCC are significantly correlated in space (Figure 1g), whereas only the first EOF for OSC and OCC are significantly correlated in space (Figure 1h). The maximum and minimum bootstrapped spatial correlations are always within 0.1 of the correlations shown in Figures 1g and 1h so we instead show the low-pass filtered envelopes of the correlations as a function of EOF number to demonstrate the contrasting ranges of correlations between EOFs. Consistent with the low predictability of OHC from OCC on seasonal time scales found by Trossman and Tyler (2022), only the first several EOFs for OCC and OHC highly correlate when a filter is not applied, but the vast majority of EOFs for OCC and OHC highly correlate when a year-long moving-average filter is applied to the OCC and OHC data (Figure 1g). Thus, it is likely that the same mechanisms that explain the variability in OHC can also explain the annual-to-longer-term variability in OCC. We investigate this further below.

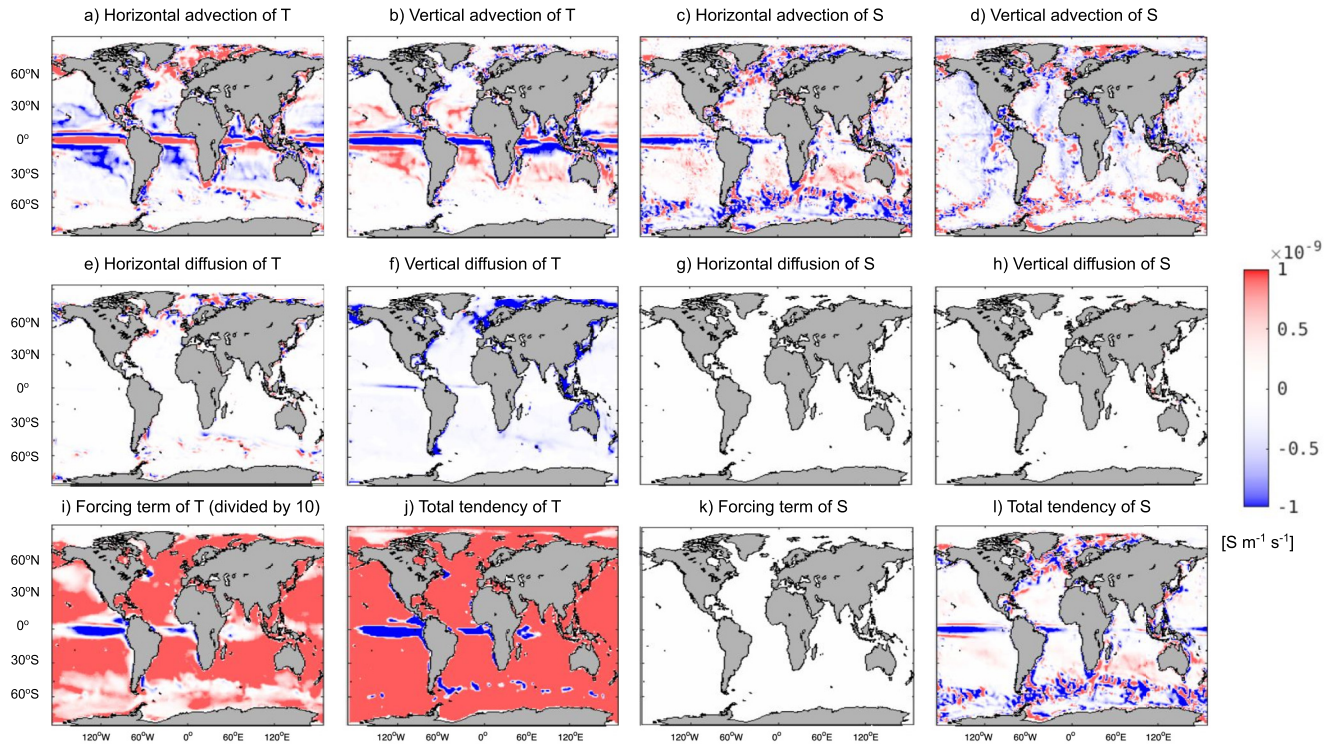

Figure 2. The depth-averaged electrical conductivity budget contributions (units in S m^{-1} s^{-1}) broken up into (a and c) horizontal advection, (b and d) vertical advection, (e and g) horizontal diffusion, (f and h) vertical diffusion, (i and k) forcing, and (j and l) total tendency terms for temperature (a and b, e and f, i and j) and salinity (c and d, g and h, k and l) terms. Note that the temperature forcing term has been divided by a factor of 10 to appear on the same colorbar scale as the other terms.

3.2. Conductivity Budget Analysis

We next decompose the electrical conductivity budget into contributions from temperature and salinity and for each of those, the depth-average of the horizontal advection, vertical advection, horizontal diffusion, vertical diffusion, forcing, and total tendency terms are shown in Figure 2. Regionally, there are large differences between the magnitudes of the temperature and salinity contributions for a given advective, diffusive, or forcing term. Consistent with expectations, the temperature forcing term tends to dominate not only the salinity forcing term but every other term in the electrical conductivity budget. However, the redistribution of electrical conductivity (or its transport) is primarily determined by the advection of both temperature and salinity. Salinity's advective contributions are larger than temperature's advective contributions in high-latitude regions and temperature's advective contributions are larger than salinity's advective contributions in low-latitude regions. The vertical advection contributions tend to be of opposite sign from the horizontal advection contributions, with the exception of salinity's advective contributions in equatorial regions. The sign is opposite between temperature's horizontal diffusion contributions and salinity's horizontal diffusion contributions in equatorial regions. The total tendency term for temperature is primarily determined by the temperature forcing term and the total tendency term for salinity is mostly set by salinity's horizontal advection term, with a net non-zero tendency when you add these two tendency terms together because there is a trend in ECCO's electrical conductivity.

We lastly present the conductivity budget tendency terms in Figure 3. We first focus on the zonally-and depth-averaged tendencies (Figure 3a). The temperature forcing term tracks the total temperature tendency term very closely over all latitudes. The temperature forcing, vertical advection of salinity, and horizontal advection of temperature contributions to the electrical conductivity dominate but are slightly offset by vertical diffusion of salinity near Antarctica. There is a trade-off of temperature forcing, vertical advection of temperature, and horizontal advection of temperature in low-latitude regions. In subpolar regions of the Northern Hemisphere, temperature forcing and vertical advection of salinity are partially offset by horizontal advection of salinity. All other terms are relatively small in their zonal and depth averages, but the diffusion terms may be underestimated, as suggested by Trossman et al. (2022). The temporal variations in the tendency terms are primarily seasonal

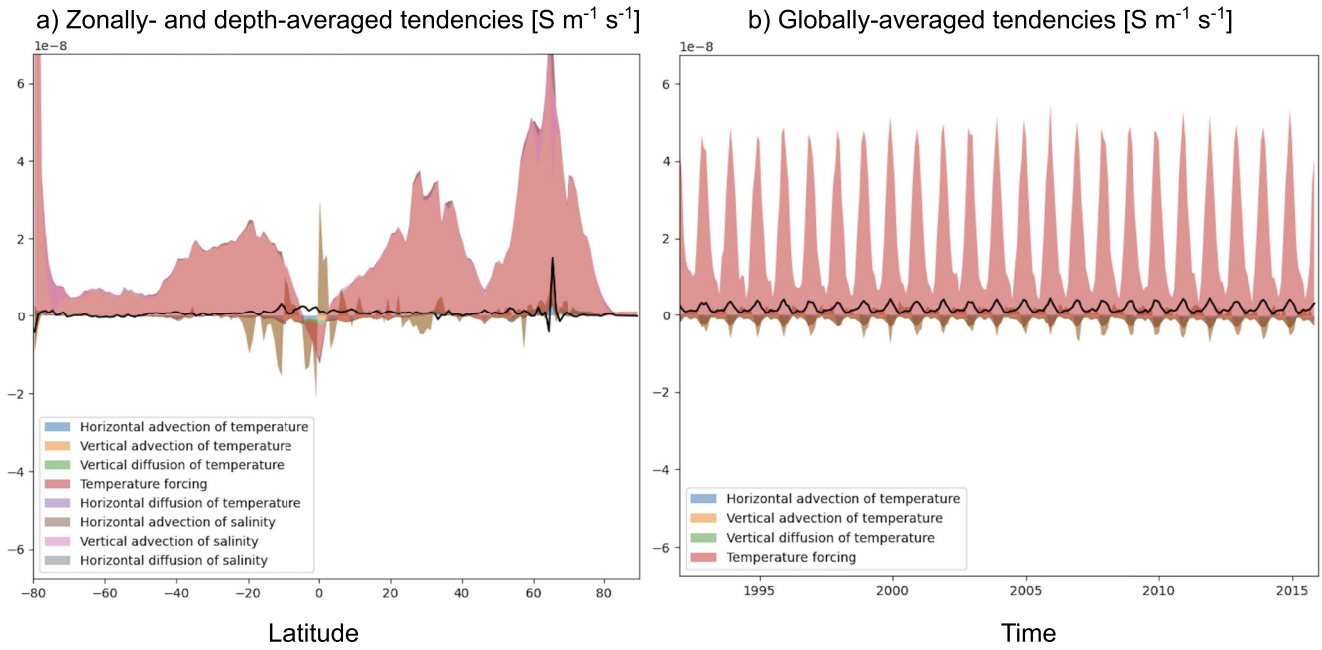

Figure 3. (Panel a) The stacked sums of the zonally- and depth-averaged electrical conductivity budget contributions (units in S m^{-1} s^{-1}) broken up into horizontal advection of temperature (blue), vertical advection of temperature (orange), horizontal diffusion of temperature (purple), vertical diffusion of temperature (green), temperature forcing (red), horizontal advection of salinity (brown), vertical advection of salinity (pink), and horizontal diffusion of salinity (gray). (Panel b) The stacked sums of the globally-averaged electrical conductivity budget contributions (units in S m^{-1} s^{-1}) broken up into a subset of the same tendency terms. The only terms shown in either panel are ones that attain values greater than 10^{-9} S m^{-1} s^{-1} at any location or time; the rest of the terms are excluded. The sum of the total tendency terms for temperature and salinity minus the temperature forcing term is indicated by the thick black curve in each panel.

with amplitudes that can be larger than the average tendencies for many terms (Figure 3b). The temperature and salinity advection tendency terms, particularly temperature's horizontal advection term, can be comparable in magnitude to the temperature forcing tendency term during July–September. The area-weighted global averages of the temporal correlations between each tendency term and the total tendencies (Table 1) reveal that only the temperature forcing tendency term is significantly positively correlated with the total electrical conductivity tendency term, but the vertical advection of salinity term is marginally anti-correlated with the total electrical conductivity tendency term, suggesting a redistributive role. The temporal correlations between the temperature forcing tendency term and the total tendency term are lower in the Arctic Ocean, consistent with lower predictability of OHC from OCC and other factors found by Trossman and Tyler (2022). Each term can be significantly correlated with the total tendency at some location in the ocean. However, the only field with both significant temporal correlations with the total tendency term (Table 1) and a non-negligible global area-weighted tendency (Figure 3b) is the temperature forcing tendency term. These findings suggest that the electrical conductivity tendencies are primarily determined by ocean heat uptake, which is consistent with the high correlation between OCC and OHC found by Trossman and Tyler (2019, 2022) given that ocean heat uptake is mostly passively advected and diffused globally, particularly outside of the Atlantic Ocean (Garuba & Klinger, 2018; Zika et al., 2021).

Table 1
The Area-Weighted Global Averages of the Pointwise Temporal Correlations Between Each of the Electrical Conductivity Budget Terms and the Total Tendency Term, Plus or Minus the Spatial Standard Deviation of the Temporal Correlations

Budget term	Correlation with total tendency term
Horiz adv T	−0.032 ± 0.10 (−0.60, 0.57)
Vert adv T	0.0062 ± 0.11 (−0.56, 0.66)
Horiz diff T	−0.0072 ± 0.11 (−0.82, 0.84)
Vert diff T	−0.061 ± 0.15 (−0.79, 0.53)
Forcing T	0.82 ± 0.35 (0.00070, 1.0)
Horiz adv S	0.014 ± 0.18 (−0.81, 0.90)
Vert adv S	−0.29 ± 0.22 (−0.99, 0.40)
Horiz diff S	0.015 ± 0.11 (−0.64, 0.74)
Vert diff S	−0.017 ± 0.092 (−0.69, 0.60)
Forcing S	0.0035 ± 0.037 (−0.50, 0.36)

Note. Also listed are in parentheses are the (minimum, maximum) values of these temporal correlations.

4. Conclusions

In the present study, we investigated the reasons for the high level of full-depth OHC predictability from full-depth OCC Trossman and Tyler (2019, 2022) that could potentially be calculated from magnetic data. We used an ocean state estimate (ECCO) to perform this analysis, which we justified by

assessing its agreement with two different observational products (one from satellites and one from in-situ data—see Supporting Information S1). We performed multiple calculations to assess the covariability between OHC and (with an EOF analysis) and to ascribe causality to specific processes (with a conductivity budget analysis).

This study provided a first long-term assessment of sea surface electrical conductivity statistics using satellite data and found good agreement with the ECCOv4r3 product. Consistent with the high level of agreement with in-situ temperature and salinity observations summarized by Heimbach et al. (2019), we found good agreement between the electrical conductivity from ECCOv4r3 and in-situ observations on a seasonal time scale. However, the agreement between ECCOv4r3 and in-situ observations degrades at deeper depths and is relatively worse below 2,000 m depth in high-latitude regions.

Lastly, we investigated why OCC and OHC are so strongly related to each other. We first demonstrated that the near-surface conductivity predominates the variability in OCC and near-surface velocities determine the variability in the horizontal gradients in OCC. We then performed EOF and electrical conductivity budget analyses. The EOF analysis suggested that the drivers of the vast majority of the variance in the OHC and OCC fields from ECCOv4r3 are similar. We further found that the temperature forcing tendency dominates the electrical conductivity budget, but the advection tendency terms can be important locally and at particular times of the year. These results suggest that the main reason why the OHC (anomaly) is highly predictable from the OCC (anomaly) is that ocean heat uptake is primarily driving the trends in electrical conductivity. This study suggests that developing the capability to monitor OCC using available observing systems (e.g., satellite magnetometry and land observatories) would be beneficial to OHC monitoring efforts.

Data Availability Statement

The data used in this study can be found at: https://doi.org/10.5281/zenodo.6834064.

Acknowledgments
The authors are grateful for the sea surface conductivity data generated by James Reagan. David S. Trossman and Robert H. Tyler were supported by the National Science Foundation, Directorate for Geosciences, OCE-2048789. The authors acknowledge the Texas Advanced Computing Center (TACC) at The University of Texas-Austin for providing High Performance Computing resources that have contributed to the research results reported here (URL: http://www.tacc.utexas.edu).

References

Adcroft, A., & Campin, J.-M. (2004). Rescaled height coordinates for accurate representation of free-surface flows in ocean circulation models. *Ocean Modelling*, *7*(3–4), 269–284. https://doi.org/10.1016/j.ocemod.2003.09.003

Adcroft, A., Hill, C., & Marshall, J. (1997). The representation of topography by shaved cells in a height coordinate model. *Monthly Weather Review*, *125*(9), 2293–2315. https://doi.org/10.1175/1520-0493(1997)125<2293:rotbsc>2.0.co;2

Campin, J.-M., Adcroft, A., Hill, C., & Marshall, J. (2004). Conservation of properties in a free surface model. *Ocean Modelling*, *6*(3–4), 221–244. https://doi.org/10.1016/s1463-5003(03)00009-x

Chaudhuri, A. H., Ponte, R. M., Forget, G., & Heimbach, P. (2013). A comparison of atmospheric reanalysis surface products over the ocean and implications for uncertainties in air-sea boundary forcing. *Journal of Climate*, *26*(1), 153–170. https://doi.org/10.1175/jcli-d-12-00090.1

Dee, D. P., Uppala, S. M., Simmons, A. J., Berrisford, P., Poli, P., Kobayashi, S., et al. (2011). The ERA-interim reanalysis: Configuration and performance of the data assimilation system. *Quarterly Journal of the Royal Meteorological Society*, *137*(656), 553–597. https://doi.org/10.1002/qj.828

Forget, G., Campin, J.-M., Heimbach, P., Hill, C. N., Ponte, R. M., & Wunsch, C. (2015). ECCO version 4: An integrated framework for nonlinear inverse modeling and global ocean state estimation. *Geoscientific Model Development*, *8*(10), 3071–3104. https://doi.org/10.5194/gmd-8-3071-2015

Forget, G., Ferreira, D., & Liang, X. (2015). On the observability of turbulent transport rates by Argo: Supporting evidence from an inversion experiment. *Ocean Science*, *11*(5), 839–853. https://doi.org/10.5194/os-11-839-2015

Fukumori, I., Wang, O., Fenty, I., Forget, G., Heimbach, P., & Ponte, R. M. (2017). *ECCO version 4 release 3*. DSpace@MIT. Retrieved from http://hdl.handle.net/1721.1/110380

Garuba, O. A., & Klinger, B. A. (2018). Ocean Heat uptake and interbasin transport of the passive and redistributive components of surface heating. *Journal of Climate*, *29*(20), 7507–7527. https://doi.org/10.1175/JCLI-D-16-0138.1

Gaspar, P., Grégoris, Y., & LeFevre, J.-M. (1990). A simple eddy kinetic energy model for simulations of the oceanic vertical mixing: Tests at station Papa and long-term upper ocean study site. *Journal of Geophysical Research*, *95*(C9), 16179–16193. https://doi.org/10.1029/jc095ic09p16179

Gent, P. R., & McWilliams, J. C. (1990). Isopycnal mixing in ocean circulation models. *Journal of Physical Oceanography*, *20*(1), 150–155. https://doi.org/10.1175/1520-0485(1990)020<0150:imiocm>2.0.co;2

Giering, R., & Kaminski, T. (1998). Recipes for adjoint code construction. *ACM Transactions on Mathematical Software*, *24*(4), 437–474. https://doi.org/10.1145/293686.293695

Gilbert, J. C., & Lemarechal, C. (1989). Some numerical experiments with variable-storage quasi-Newton algorithms. *Mathematical Programming*, *45*(1–3), 407–435. https://doi.org/10.1007/bf01589113

Griewank, A. (1992). Achieving logarithmic growth of temporal and spatial complexity in reverse automatic differentiation. *Optimization Methods and Software*, *1*(1), 35–54. https://doi.org/10.1080/10556789208805505

Heimbach, P., Fukumori, I., Hill, C. N., Ponte, R. M., Stammer, D., Wunsch, C., et al. (2019). Putting it all together: Adding value to the global ocean and climate observing systems with complete self-consistent ocean state and parameter estimates. *Frontiers in Marine Science*, *6*, 55. https://doi.org/10.3389/fmars.2019.00055

Heimbach, P., Menemenlis, D., Losch, M., Campin, J. M., & Hill, C. (2010). On the formulation of sea-ice models. Part 2: Lessons from multi-year adjoint sea ice export sensitivities through the Canadian Arctic Archipelago. *Ocean Modelling*, *33*(1–2), 145–158. https://doi.org/10.1016/j.ocemod.2010.02.002

Irrgang, C., Saynisch, J., & Thomas, M. (2019). Estimating global ocean heat content from tidal magnetic satellite observations. *Nature Scientific Reports*, *9*(1), 7893. https://doi.org/10.1038/s41598-019-44397-8

Kuvshinov, A. V. (2008). 3-D global induction in the oceans and solid Earth: Recent progress in modeling magnetic and electric fields from sources of magnetospheric, ionospheric and oceanic origin. *Surveys in Geophysics*, *29*(2), 139–186. https://doi.org/10.1007/s10712-008-9045-z

Large, W. G., & Yeager, S. G. (2009). The global climatology of an interannually varying air-sea flux data set. *Climate Dynamics*, *33*(2–3), 341–364. https://doi.org/10.1007/s00382-008-0441-3

Losch, M., Menemenlis, D., Campin, J. M., Heimbach, P., & Hill, C. (2010). On the formulation of sea-ice models. Part 1: Effects of different solver implementations and parameterizations. *Ocean Modelling*, *33*(1–2), 129–144. https://doi.org/10.1016/j.ocemod.2009.12.008

Manoj, C., Kuvshinov, A., Maus, S., & Luhr, H. (2006). Ocean circulation generated magnetic signals. *Earth Planets and Space*, *58*(4), 429–437. https://doi.org/10.1186/bf03351939

McDougall, T. J., & Barker, P. M. (2011). *Getting started with TEOS-10 and the Gibbs Seawater (GSW) oceanographic toolbox* (p. 28). SCOR/IAPSO WG127.

Menemenlis, D., Hill, C., Adcrocft, A., Campin, J. M., Cheng, B., Ciotti, B., et al. (2005). NASA supercomputer improves prospects for ocean climate research. *Eos, Transactions American Geophysical Union*, *86*(9), 95–96. https://doi.org/10.1029/2005eo090002

Nocedal, J. (1980). Updating quasi-Newton matrices with limited storage. *Mathematics of Computation*, *35*(151), 773–782. https://doi.org/10.1090/s0025-5718-1980-0572855-7

Palter, J. B., Griffies, S. M., Samuels, B. L., Galbraith, E. D., Gnanadesikan, A., & Klocker, A. (2014). The deep ocean buoyancy budget and its temporal variability. *Journal of Climate*, *27*(2), 551–573. https://doi.org/10.1175/jcli-d-13-00016.1

Paulson, C. A., & Simpson, J. J. (1977). Irradiance measurements in the upper ocean. *Journal of Physical Oceanography*, *7*(6), 952–956. https://doi.org/10.1175/1520-0485(1977)007<0952:imituo>2.0.co;2

Piecuch, C. G., & Ponte, R. M. (2011). Mechanisms of interannual steric sea level variability. *Geophysical Research Letters*, *38*(15), L15605. https://doi.org/10.1029/2011GL048440

Piecuch, C. G., & Ponte, R. M. (2014). Mechanisms of global-mean steric sea level change. *Journal of Climate*, *27*(2), 824–834. https://doi.org/10.1175/jcli-d-13-00373.1

Pilo, G. S., Oke, P. R., Coleman, R., Rykova, T., & Ridgway, K. (2018). Impact of data assimilation on vertical velocities in an eddy resolving ocean model. *Ocean Modelling*, *131*, 71–85. https://doi.org/10.1016/j.ocemod.2018.09.003

Reagan, J. R., Zweng, M. M., Seidov, D., Boyer, T. P., Locarnini, R. A., Mishonov, A. V., et al. (2019). *World ocean Atlas 2018, volume 6: Conductivity*. In A. Mishonov Technical Editor (Eds.), *NOAA Atlas NESDIS* (Vol. 86, pp. 38).

Redi, M. H. (1982). Oceanic isopycnal mixing by coordinate rotation. *Journal of Physical Oceanography*, *12*(10), 1154–1158. https://doi.org/10.1175/1520-0485(1982)012<1154:oimbcr>2.0.co;2

Sanford, T. B. (1971). Motionally induced electric and magnetic fields in the sea. *Journal of Geophysical Research*, *76*(15), 3476–3492. https://doi.org/10.1029/JC076i015p03476

Stammer, D., Balmaseda, M., Heimbach, P., Köhl, A., & Weaver, A. (2016). Ocean data assimilation in support of climate applications: Status and perspectives. *Annual Review of Marine Science*, *8*(1), 491–518. https://doi.org/10.1146/annurev-marine-122414-034113

Stephenson, D., & Bryan, K. (1992). Large-scale electric and magnetic fields generated by the oceans. *Journal of Geophysical Research*, *97*(C10), 15467. https://doi.org/10.1029/92jc01400

Trossman, D. S., & Tyler, R. H. (2019). Predictability of ocean heat content from electrical OCC. *Journal of Geophysical Research: Oceans*, *124*, 667–679. https://doi.org/10.1029/2018JC014740

Trossman, D. S., & Tyler, R. H. (2022). A prototype for remote monitoring of ocean heat content anomalies. *Journal of Atmospheric and Oceanic Technology*, *39*(5), 667–688. https://doi.org/10.1175/JTECH-D-21-0037.1

Trossman, D. S., Whalen, C., Haine, T. W. N., Waterhouse, A. F., Bigdeli, A., Nguyen, A. T., et al. (2022). Tracer and observationally derived constraints on diapycnal diffusivities in an ocean state estimate. *Ocean Science*, *18*(3), 729–759. https://doi.org/10.5194/os-18-729-2022

Tyler, R. H. (2017). *Mathematical modeling of electrodynamics near the surface of Earth and planetary water worlds*. Technical Report TM-2017-219022, *NASA*. Retrieved from https://ntrs.nasa.gov/citations/20170011279

Tyler, R. H., Boyer, T. P., Minami, T., Zweng, M. M., & Reagan, J. R. (2017). Electrical conductivity of the global ocean. *Earth Planets and Space*, *69*(1), 156. https://doi.org/10.1186/s40623-017-0739-7

Tyler, R. H., Maus, S., & Luhr, H. (2003). Satellite observations of magnetic fields due to ocean tidal flow. *Science*, *299*(5604), 239–241. https://doi.org/10.1126/science.1078074

Tyler, R. H., Sanford, T. B., & Oberhuber, J. M. (1997). Geophysical challenges in using large-scale ocean-generated EM fields to determine the ocean flow. *Journal of Geomagnetism and Geoelectricity*, *49*(11–12), 1351–1372. https://doi.org/10.5636/jgg.49.1351

UNESCO. (1985). The international system of units (SI) in oceanography. *Science*, *45*, 124. Technical Paper in Marine.

Wang, G., Zhao, C., Zhang, M., Zhang, Y., Lin, M., & Qiao, F. (2020). The causality from solar irradiation to ocean heat content detected via multi-scale Liang–Kleeman information flow. *Scientific Reports*, *10*(1), 17141. https://doi.org/10.1038/s41598-020-74331-2

Weaver, A. T., & Courtier, P. (2001). Correlation modeling on a sphere using a generalized diffusion equation. *The Quarterly Journal of the Royal Meteorological Society*, *127*(575), 1815–1846. https://doi.org/10.1002/qj.49712757518

Wunsch, C., & Heimbach, P. (2007). Practical global oceanic state estimation. *Physica D*, *230*(1–2), 197–208. https://doi.org/10.1016/j.physd.2006.09.040

Zika, J. D., Gregory, J. M., McDonagh, E. L., Marzocchi, A., & Clément, L. (2021). Recent water mass changes reveal mechanisms of ocean warming. *Journal of Climate*, *34*(9), 3461–3479. https://doi.org/10.1175/JCLI-D-20-0355.1

References From the Supporting Information

Grayver, A. V. (2021). Global 3-D electrical conductivity model of the world ocean and marine sediments. *Geochemistry, Geophysics, Geosystems*, *22*, e2021GC009950. https://doi.org/10.1029/2021GC009950

Irrgang, C., Saynisch-Wagner, J., & Thomas, M. (2018). Depth of origin of ocean-circulation-induced magnetic signals. *Annales Geophysicae*, *36*, 167–180. https://doi.org/10.5194/angeo-36-167-2018

Reul, N., Grodsky, S. A., Arias, M., Boutin, J., Catany, R., Chapron, B., et al. (2020). Sea surface salinity estimates from spaceborne L-band radiometers: An overview of the first decade of observation (2010–2019). *Remote Sensing of Environment*, *242*, 111769. https://doi.org/10.1016/j.rse.2020.111769